

A transparent two-dimensional *in situ* beam-position and profile monitor for synchrotron X-ray beamlines

Nicholas R. Kyele,^a Klaas Decanniere^{b,c} and Roelof G. van Silfhout^{a*}

^aSchool of Electrical and Electronic Engineering, The University of Manchester, PO Box 88, Manchester M60 1QD, UK, ^bDUBBLE at ESRF, Polygone Scientifique Louis Néel, 6 rue Jules Horowitz, 38000 Grenoble, France, and ^cVrije Universiteit Brussel, Belgium.
E-mail: r.vansilfhout@manchester.ac.uk

A compact, inexpensive and easy-to-construct two-dimensional *in situ* beam-position and profile monitor for synchrotron X-ray beamlines is presented. The device is based on the collection of spatially resolved scattered radiation from a polyimide foil. The X-ray beam passes through a foil placed in the path of the beam, which absorbs no more than 3% of the beam at 12 keV. The scattered radiation is collected at an angle of 90° through a collimator located below the foil onto a CCD sensor. The device was tested on bending-magnet beamline BM26 at the ESRF synchrotron radiation source and has a positional sensitivity better than 10 µm with a large working range of 25 mm × 25 mm. Although the device is optimized for use in the range 10–12 keV, it can easily be modified for use with higher-energy beams by using a suitably chosen scattering foil.

© 2005 International Union of Crystallography
Printed in Great Britain – all rights reserved

Keywords: X-rays; beam-position monitor; beam-profile monitor; CCD-based; detectors.

1. Introduction

Third-generation synchrotron radiation sources have introduced smaller and higher-intensity X-ray beams than available from earlier-generation sources. These highly collimated beams are routinely used on micrometre-sized samples. Although beam stability at third-generation sources has improved significantly, it is very difficult to remove beam drifts that are of the order of micrometres. Beam position changes may be caused by many sources, including refilling of the storage ring, thermal cycles of the monochromators, mirrors and other temperature-, pressure- and mechanical-related factors which may lead to loss of focus on the sample or result in the beam missing the sample altogether.

Various devices based on different methods have been studied including, but not limited to, photoconductive, photoemissive, fluorescence and elastic scattering-based devices. Photoconductive devices (Sakae *et al.*, 1997; Bergonzo *et al.*, 1999; Schulze-Briese *et al.*, 2001) which use carriers generated within diamond foils to produce current have been promising with sensitivities of 2–3 µm. Diamond provides a transparent and radiation hard medium that does not melt under intense beam exposure. However, these diamond photodiodes have been studied for energy ranges of below 5 keV (Bergonzo *et al.*, 1999) with up to 22% of the beam absorbed by the devices. Subsequent diamond foil models have overcome these problems only to be limited by a small linear working range of ±1 mm caused by saturation of the

current in the foil after a few millimetres (Sakae *et al.*, 1997). Silicon photodiode models based on direct illumination (van Silfhout, 1998) of the X-ray beam are not suitable for long-term use since they tend to become damaged after long exposure. Blade-based photoemissive devices that measure the scattered photoelectrons from metal blades (Chen *et al.*, 1998) have shown sensitivities down to 1 µm. Fluorescence devices which measure photons from metal foils (Alkire *et al.*, 2000) have demonstrated equal sensitivity but have proven to be affected by scattered radiation from the kapton, Mylar and beryllium windows of the beamlines since they do not discriminate incoming photons. Metal foils are not recommended for spectroscopic experiments as there would clearly be anomalies at the $K\alpha$ and $K\beta$ wavelengths. The split ion chamber method (Koyama *et al.*, 1989; Schildkamp & Pradervand, 1995) has shown relatively good sensitivities to narrow beams but requires two devices for simultaneous horizontal and vertical position monitoring. Most of the existing devices mentioned concentrate only on beam positioning and not profile monitoring.

Several beam-profile monitors based on detection of ions generated by the X-ray beam from either residual gases in the beam path or from specially introduced gas have been reported. For example, a gas sheet model (Hashimoto *et al.*, 2002) based on the collection of ions from a high-pressure oxygen sheet has given acceptable profiles, but the size of the equipment and mechanics used limit its usefulness in already existing and operational beamlines which have limited hutch

space. Devices which use residual gas (Ioudin *et al.*, 1998; Artemiev *et al.*, 2002) seem promising but the requirement on the relatively high residual gas pressure of 1 mPa will limit their use.

Charge coupled devices (CCDs) have been the choice of preference for various studies and also for general use in operational beamlines. One of the commercially available two-dimensional beam-position and profile monitors is the X-ray Eye (Photonic Science, UK; <http://www.photonic-science.co.uk>) that is based on direct irradiation of the X-ray beam onto the CCD sensor. This translates to total absorption of the beam and is therefore only useful for beam positioning before experiment set-up. A second CCD-based profile monitor designed at the ESRF (SESO XBM X-ray beam monitor; <http://www.seso.com>) is now commercially available. However, for both detectors, placement in the path of the beam excludes them as an *in situ* monitor.

In this article we present a low-cost CCD-based device that is used simultaneously as a two-dimensional beam-position monitor and a beam-profile monitor. Our device works on the principle of collection of spatially resolved scattered radiation from a thin foil (van Silfhout, 1999). A thin polyimide foil is placed in the path of the beam and this absorbs no more than 3% of the beam (see Fig. 1) at 12.6 keV to generate the scattered radiation that is amplified by a suitable fluorescent phosphor film. The radiation is collected at an angle of 90° to the direction of the beam ensuring that there is no direct exposure with the beam and is therefore suited for long-term operation. Owing to its very low beam absorption, the device is particularly suited for permanent *in situ* beam monitoring and can easily be introduced in existing beamlines. Here we report on preliminary measurements performed at a bending-magnet source with monochromatic radiation of 12.6 keV. Compared with insertion-device (ID) beamlines, a bending magnet has several orders of magnitude less intensity and a much larger footprint and presents therefore a challenging test for our device.

2. Design and principle of operation

The beam-position and profile monitor measures spatially resolved scattered radiation from a polyimide foil (kapton, $C_{22}H_{10}N_2O_5$) using a CCD sensor. A schematic of the device is shown in Fig. 2.

The foil, with a thickness of $127\ \mu\text{m}$, is positioned at an inclined angle α of 45° . This angle of inclination determines the size of the footprint of the beam on the foil and offers an elegant way of increasing resolution. For a given angle α , the size of the footprint is increased by a factor of $1/\sin\alpha$. Similarly, the size of the beam in the x direction is magnified by inclining the sensor and scintillator at an angle β . This arrangement has two advantages. First, it increases the spatial resolution or, in other words, the resolution of beam profiling (imaging). This is particularly important for focused beams that have a size very similar to that of individual CCD detector pixels. Secondly, the positional sensitivity is also improved for tilt angles smaller than 45° by a factor of $(\tan\alpha)^{-1}$. Likewise,

the tilt angle β of the sensor can be made flexible and this will result in the spreading out of the beam in the x direction on the sensor. In these initial experiments, both α and β were fixed to 45° and 0° , respectively.

In previous experiments, metal foils were used as the source of scattering (van Silfhout, 1999) but in this case a kapton foil was preferred owing to its amorphous nature and hence random scattering of the X-ray photons without any diffraction. The scatter foil absorbs no more than 3% of the beam at 12 keV. At higher X-ray energies the absorption becomes negligible.

In order to image the footprint of the beam on the scattering foil, we have to use a collimator (also called a 2-D Soller slit) because there is no suitable lens available for X-ray photons. The collimator is positioned at a scattering angle of 90° . This scattering geometry ensures that no high-intensity forward and backscattered X-rays are collected. The scattered

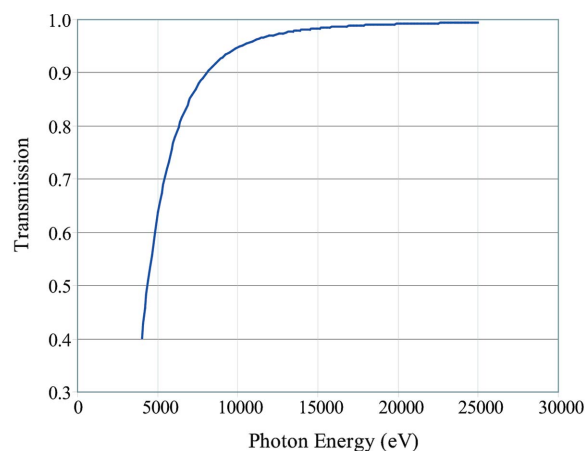


Figure 1 Transmission curve of a $127\ \mu\text{m}$ -thick kapton foil. At 12 keV, only 3% of the beam is absorbed making it suitable for *in situ* beam-position and profile monitoring.

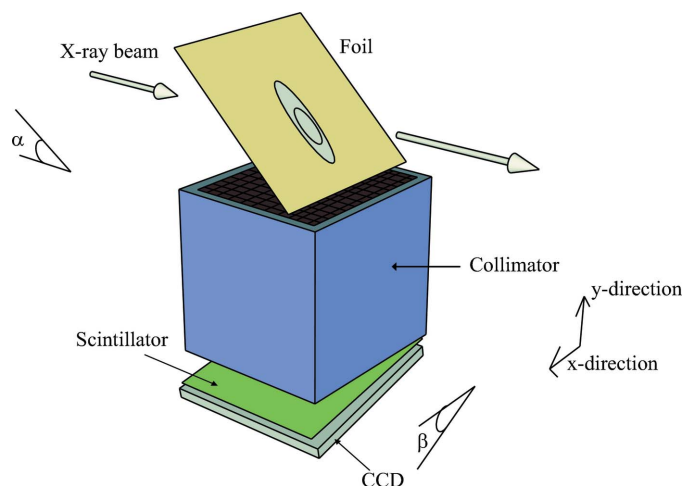


Figure 2 Schematic of the X-ray beam monitor. The X-ray beam hits a polyimide foil tilted at an angle α . The scattered radiation from the foil is collected at 90° through the collimator onto the scintillator. By reducing tilt angles α and β , the positional sensitivity and spatial resolution of the device is increased.

radiation that passed through the collimator is collected by a high-resolution CCD imager (EEV CCD05-30 series). The collimator is assembled from 24 aluminium spacers and 23 copper meshed foils each placed on top of the other. The foils are 0.1 mm thick whereas the spacers are 2 mm thick (see Fig. 3). The collimator is held together by four screws making it about 50 mm long including mechanical tolerance. To study the effect of collimator resolution on the accuracy of the beam position, two collimators with different hole sizes were used; one with a $400\ \mu\text{m} \times 400\ \mu\text{m}$ square hole size with a track width of $100\ \mu\text{m}$ (collimator-S) and one with a $1000\ \mu\text{m} \times 1000\ \mu\text{m}$ square hole size with a track width of $125\ \mu\text{m}$ (collimator-L). The meshed copper foils are chemically etched with a manufacturing tolerance of $25\ \mu\text{m}$. For both collimators, the size of the mesh is $25\ \text{mm} \times 25\ \text{mm}$ and the area of the whole foil and spacer is $50\ \text{mm} \times 50\ \text{mm}$. A drawing of the foil and a photograph of the collimator of our device are shown in Figs. 3(a) and 3(b), respectively.

The selection of a hole size is a trade-off between intensity and resolution. A larger hole means more intensity is collected but accuracy is lost as the hole size becomes much larger than the CCD pixel size. We chose foils with a thickness of $100\ \mu\text{m}$ because thinner foils lack rigidity and would introduce complications in the assembly of the collimator. The width of the tracks is dominated by the manufacturing process; the minimum feature size obtainable reproducibly through chemical etching is equal to the foil thickness. To keep costs low and for ease of etching, copper foil was selected. Ideally, heavier metals such as molybdenum and lead with better

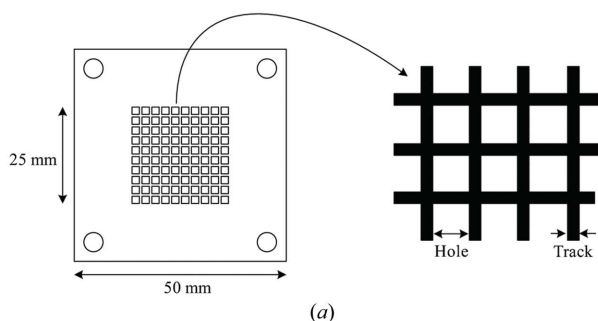
absorbing properties and less fluorescence for this particular energy range should be used.

Owing to mechanical restrictions, the collimator is held about 7.5 mm above the CCD. Ideally, the collimator would be mounted directly onto the CCD. At this height, the potential overlap of X-rays exiting from neighbouring collimator holes is $59\ \mu\text{m}$ which is less than the track width of $100\ \mu\text{m}$ for collimator-S ($80\ \mu\text{m}$, and $125\ \mu\text{m}$ for collimator-L). The same principle applies at the top of the collimator with regard to the photons emitted from the footprint of the beam on the foil, and, to maintain an overlap ratio of 0.25 or less at the top of the collimator, the scatter foil is held 15 mm above the collimator.

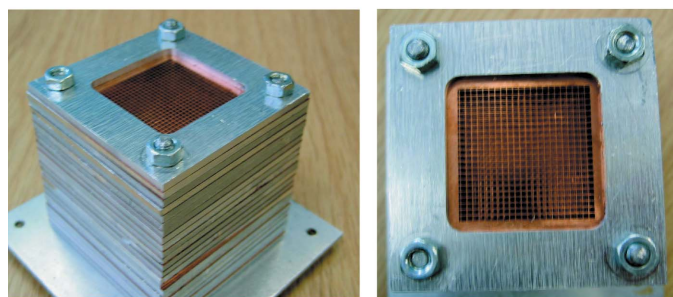
Since the CCD used is not radiation hard, the scattered radiation from the collimator is converted into the visible range through a gadolinium oxysulfide (GOS) based scintillating foil. The fluorescent foil is in direct contact with a fibre optic plate which is attached to the CCD and which has a native resolution matching the CCD. The GOS-based scintillator was chosen because its emission wavelength ($510\ \text{nm}$) closely matches the spectral response (EEV Limited, 1999) of the CCD, which has a quantum efficiency of 35% at $550\ \text{nm}$.

The CCD has a usable resolution of 1242×1152 (with a pixel size of $22.5\ \mu\text{m}$) plus dummy pixels giving it a full readable resolution of 1296×1168 . As is common with CCDs, the data are read out serially and subsequently digitized into 16-bit numbers through a single hybrid analog-to-digital converter. The image is transferred to the host computer through a parallel data interface. Owing to the limitations of the electronics, the readout time of the CCD was limited to 5 s. For all experiments we opted for an exposure time of 10 s. This gives a frame rate of four frames per minute.

To operate the CCD at the required temperature, the CCD is cooled using a Peltier cooling system to 243 K. The collimator, scintillator, CCD and Peltier cooler are situated in a vacuum chamber in order to avoid condensation. Scattered X-ray radiation can pass through a small hole in the chamber that is covered by a thin film of black Mylar which stops visible light from entering the detector.



(a)



(b)

Figure 3

(a) The structure of a copper foil with a chemically etched mesh is shown. The hole, track and thickness dimensions are $400\ \mu\text{m}$, $100\ \mu\text{m}$, $100\ \mu\text{m}$, respectively, for collimator-S and $1000\ \mu\text{m}$, $125\ \mu\text{m}$, $125\ \mu\text{m}$, respectively, for collimator-L. (b) The collimator is clamped by four screws and is then placed directly over the CCD sensor. The foils have been tightly aligned to within an error of $25\ \mu\text{m}$.

3. Test

The performance tests for our device were carried out on the bending-magnet beamline branch BM26A at the ESRF source. This beamline is dedicated to EXAFS and protein crystallography studies. The beamline uses a water-cooled sagittal-focusing Si(111) crystal monochromator tunable over an energy range of 5–30 keV. For our experiments the EXAFS platform of the beamline was used situated 31 m from the source. The beam was set at 12.66 keV and focused to a spot of size $0.5\ \text{mm} \times 0.5\ \text{mm}$ with a flux of approximately $10^{11}\ \text{photons s}^{-1}$ (Borsboom *et al.*, 1998) using two Si(111) mirrors. The platform rested on a motorized linear stage that moved the device perpendicular to the direction of travel of the beam.

The scatter foil was placed in air close to the sample position and was held in place with an aluminium foil holder set at a fixed angle of 45° .

4. Results

Given that the pixel size of the CCD is much smaller than the hole size of both collimators, the image from the detector was binned using a 2×2 format at the hardware level. In the binning process, the charge of neighbouring pixels is added. This is a noise-free process because the addition is performed on the CCD sensor. In our tests, the binning resolution was limited by software but can be adjusted to accommodate more pixels. The CCD electronics allowed a maximum binning of 2×2 that resulted in an image with a resolution of 648×584 binned pixels. For convenience, we shall from now on use the word pixel when we refer to *binned* pixels. Before every set of tests, a 'dark' image was taken with the beam off, which is later subtracted from the main image to remove the background operating noise of the CCD. For consistency, the dark image is taken at the same temperature and exposure settings as the test images, for every set of tests. This is not necessary for every test since the temperature and readout conditions remained fairly constant for the whole of the test time. Using collimator-S, the image obtained from the CCD (see Fig. 4) is then reduced to the resolution of the collimator. This is done by grouping bunches of pixels into super pixels; each super pixel holds the sum of the intensity of a group of pixels equal to the size of a hole in the collimator. For example, in the case of collimator-S a super pixel represents a group of 9×9 pixels. The pixels that lie under the tracks of the collimator are discarded. This in effect reduces the full-size image to the resolution of the collimator, in this case from 648×584 to 58×53 for collimator-S. The same principle applies for collimator-L. The horizontal and vertical profiles of the beam are then obtained by adding the rows and columns of the image, respectively. Fig. 5 illustrates the vertical and horizontal profiles of the beam.

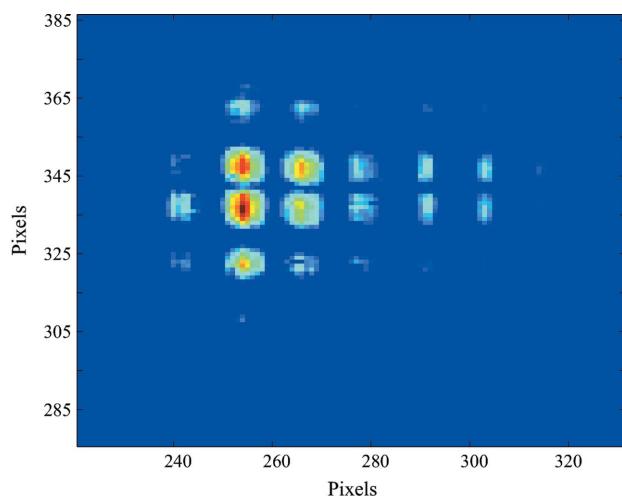


Figure 4
An enlarged 2×2 binned image from the CCD taken with collimator-S.

The full width at half-maximum (FWHM) of the beam profiles in the horizontal and vertical direction were determined by fitting the data with a Gaussian (see Fig. 5). The horizontal and vertical FWHMs were found to be $889 (\pm 29) \mu\text{m}$ and $484 (\pm 93) \mu\text{m}$, respectively, taking into account correction for tilt angle α in the vertical profile. These values represent the beam widths broadened by the instrument response function that is dominated by the collimator hole size. Given the nature of the bending-magnet source, the focused beam is actually elliptical in nature, being wider in the horizontal direction than in the vertical, as reflected by the measured values.

For comparison the beam profile in the vertical direction was measured independently using a direct exposure of a diode array with the X-ray beam (see Fig. 6). This diode array consists of a large number of separate diodes of height $100 \mu\text{m}$ and width 10 mm . The full curve in Fig. 6 represents the best-fit Gaussian to the data and has a FWHM of $480 \mu\text{m}$.

To establish the positional sensitivity of our device, the linear actuator was moved in small steps of 10 , 50 and $100 \mu\text{m}$ vertically in the plane perpendicular to the direction of travel of the beam. In these tests we assume that the beam itself does not move. To determine the width and centre of mass of the beam, a Gaussian was fitted on the profiles (see Fig. 5) using a least-squares fitting algorithm based on a combination of the Levenberg–Marquardt and Gaussian–Newton methods. The fitted data were generated to 95% confidence bounds (equivalent to ± 1 standard deviation), the goodness-of-fit (GOF) parameter of the *Matlab* mathematical package.

Fig. 7 illustrates the vertical profile response of the device to $10 \mu\text{m}$ and $100 \mu\text{m}$ steps, using collimator-S. From these data we conclude that our device can accurately track beam movement to at least $10 \mu\text{m}$. Owing to the limited movement of the linear system in the horizontal direction, calibration in

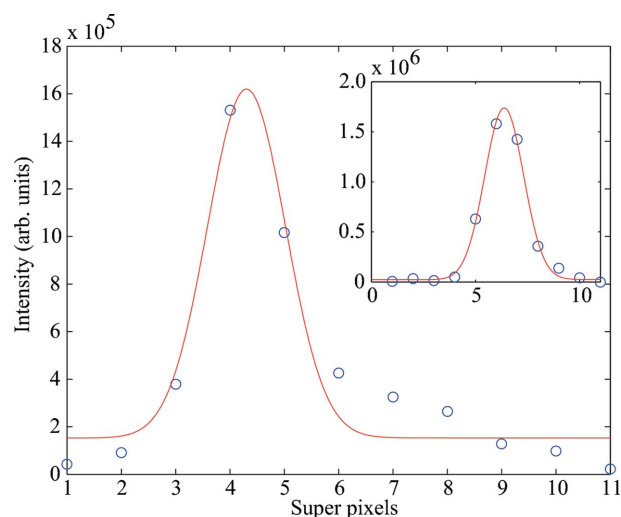


Figure 5
The vertical and horizontal (inset) profiles of the X-ray beam as measured with collimator-S. Each data point represents the intensity of a super pixel. Here, super pixels consist of groups of CCD pixels and reduce the measured image to the resolution of collimator-S. The solid curves represent best-fit Gaussian profiles which are used to determine the width and centre position of the beam.

similar small steps in this axis could not be performed. However, from the horizontal profile of the beam obtained from the vertical step movements and subsequent centre of the fit, we would expect that there would be no change in the horizontal profile and the centre of the fit would remain fixed. For the full range of 200 μm (see Fig. 7 inset), the change in the centre fit of the horizontal profile was less than 5 μm .

The exact same steps were measured using both collimator-S and collimator-L for comparison and, as expected, collimator-S with the higher resolution resulted in more accurate centre fits. The GOF statistics are summarized in Table 1, with

$$R^2 = 1 - \left\{ \frac{\sum_{i=1}^n [y_{(i)m} - y_{(i)f}]^2}{\sum_{i=1}^n [y_{(i)m} - \bar{y}]^2} \right\}.$$

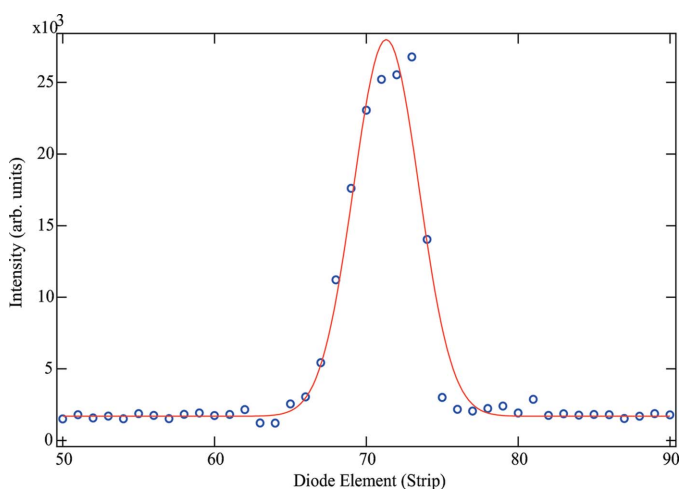


Figure 6
The vertical profile of the beam as measured by placing a linear photodiode array in the X-ray beam. Each diode element is 100 μm high and 10 mm wide. The full curve represents the best-fit Gaussian curve to the data.

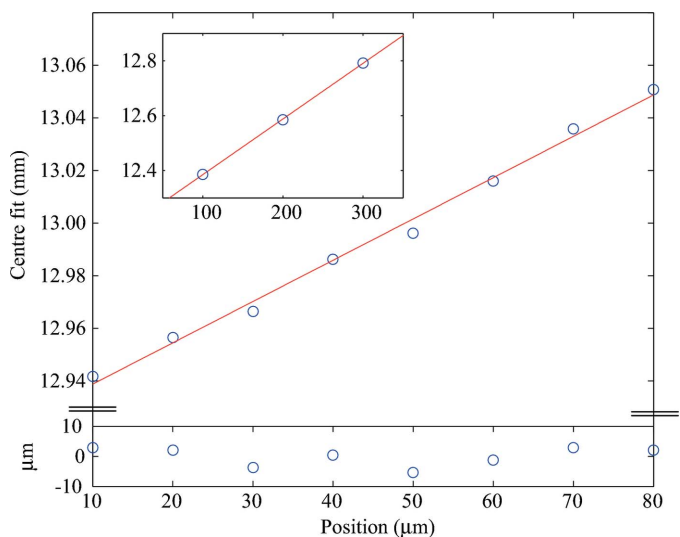


Figure 7
The positional sensitivity of the device is measured by moving the device through the beam in steps of 10 μm and 100 μm (inset) in the vertical direction. The lower panel shows the best-fit residues.

Table 1
GOF statistics for the vertical profile calibration of the device for various steps.

Steps (μm)	R^2	
	Collimator-S	Collimator-L
10	0.9933	0.9872
50	0.9999	0.9857
100	0.9998	0.9887

The GOF statistic used to test the quality of the fitted data $y_{(i)f}$ from the measured data $y_{(i)m}$ in this case was the R^2 -test which is very close to its ideal value of 1. Here, \bar{y} represents the mean of the measured data.

For a better understanding of the intensity collected by the sensor and the response of the CCD detector, images were taken from the scatter foil without any of the collimators (see Fig. 8). The images were taken under the same temperature and exposure-time conditions as the images with the collimators. Comparison of this intensity value with the intensity collected under collimator-S (Fig. 8 inset) shows a difference of at least two orders of magnitude. With the source point on the scattering foil several centimetres away from the CCD one would expect a uniform exposure in the measurement without any collimator assuming that the scattering foil is amorphous. Some anomalies are present in the measurement especially near the perimeter of the chip, which is related to damage to the scintillator foil. The slight slope of the line is because the exposure is not interrupted upon readout. Owing to the nature of the readout of the CCD, some pixels are exposed slightly longer than others.

A series of small peaks (or fringing) is seen in the data taken with the collimator (see inset of Fig. 8) on either side of the main peaks (located between pixels 300 and 400). Ideally, the collimator would consist of capillary-like columns drilled

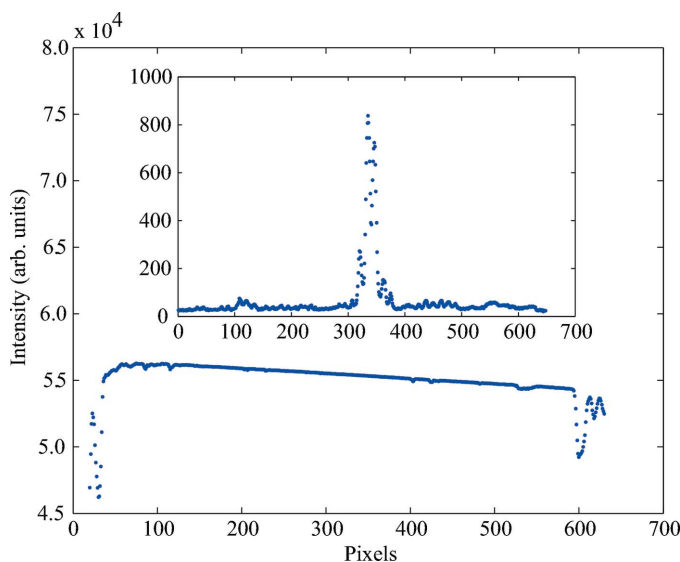


Figure 8
Comparison of scattered radiation collected with (inset) and without the collimator. The readings were taken from the same scatter foil under similar temperature and exposure settings.

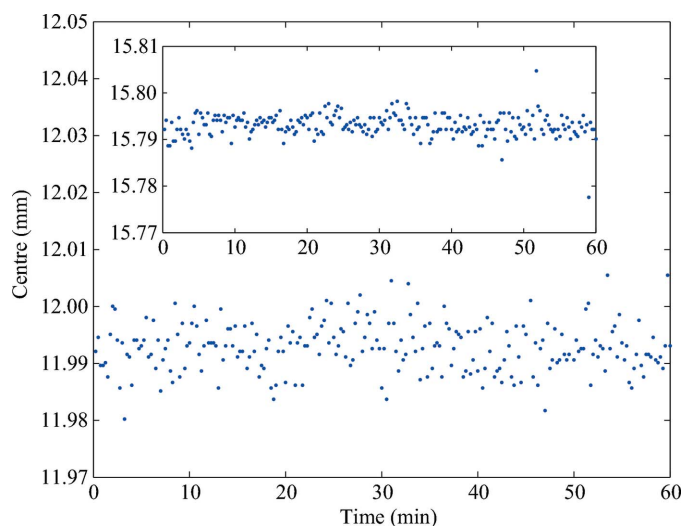


Figure 9
Time runs showing vertical and horizontal (inset) swings of the focused beam. Maximum swings were 20 μm and 10 μm , respectively.

from a solid block that would precisely resolve the scattered radiation. From our collimator, the design allows radiation scattered at certain non-vertical angles to travel from the source through the meshed foils onto the sensor, thus causing these fringes. This effect can further be used to enhance the resolution of the device as a profile monitor (to be published).

To study the stability and performance of the device as a position monitor over long periods, time-scan runs of 60 min were carried out. Since our readout time was limited to 5 s, the exposure time was set to 10 s, though the device can handle exposure times down to 1 ms provided the readout time of the CCD is improved. This gave readings at intervals of 15 min. Fig. 9 shows that the beam is relatively stable with maximum swings of 20 μm in the vertical direction with relatively smaller 10 μm swings in the horizontal direction.

5. Discussion

The detection of diffusely scattered radiation from a thin polyimide foil has been shown to be effective in the measurement of both beam position and profile albeit at low sample rates. Currently, the sample rate is limited by the readout electronics of the CCD system used. Ideally, a binning ratio would be used which matches the resolution of the image to that of the collimator. This would reduce exposure and data acquisition time to well below 50 ms. The experiments were conducted in a non-vacuum environment on a bending-magnet source. Air absorption and air scatter have been neglected in the analysis of the data but, given the good results obtained, we can safely assume that, under vacuum operating conditions and with higher intensity sources, similar and even better data quality can be produced. Once the image had been obtained from the CCD and the subsequent profiles, a simple well known Gaussian fitting technique was selected, which gives a good fitting in a few iterations thus making the processing time negligible compared with the drift of the beam. The GOF of the data is also quickly checked with

standard statistical methods. It is due to this careful analysis of the changes in relative intensity of the adjacent super pixels that positional sensitivity of sub-pixel resolution is achieved.

The principle of measurement of elastically scattered radiation makes the device suitable for several types of beamlines and for both focused and unfocused beams. There are three basic device parameters to target a particular beamline resulting in optimum performance. They are the type and thickness of the scatter foil, the collimator hole size and the type and thickness of the scintillator foil. For example, a high-energy wiggler-type beamline would use a thicker and heavier scintillator foil to convert a higher percentage of scattered photons into visible light. In addition, a thicker scatter foil could be used, made of a heavier element.

From this study performed at a bending-magnet beamline it is clear that for devices aimed at ID beamlines one should select a significantly smaller collimator hole size. Typically, ID beamlines have intensities of two to three orders higher compared with a bending-magnet beamline, and a collimator with a hole size one order of magnitude smaller than presented here would provide similar intensities as measured in this study. The use of tenfold smaller hole sizes will improve positional sensitivity to sub-micrometre levels and enhance the resolution of the beam image drastically. These collimators can be manufactured using alternative technology such as fibre optic capillary arrays that feature hole sizes of 50 μm or less.

The linear range of the device is only limited by the CCD size and can be used for position monitoring of relatively long distances compared with other devices with no loss of sensitivity. This capability is particularly useful if one would like to observe the changes in beam profile in the process of focusing a beam. The low absorption factor permits the use of multiple devices on the same beamline at different locations for better positioning.

The whole process of image analysis, profile derivation and centre fit can be optimized for implementation on a fast hardware platform. Field programmable gate array devices running in embedded systems can quickly read out an image at many frames per second while deriving the beam position and profile without the need for external computational hardware. These embedded systems can subsequently be paired with a control system to correct the position of the beam and/or the sample stage.

Monolithic active pixel sensors (MAPS) based on complementary metal oxide semiconductor (CMOS) technology have megapixel resolution and can be read in about 100 ms (1024×1024 pixels read at 10 MHz). The big advantage of such devices over CCDs is that a small area can be read out much faster; for example, a 100×100 image would be read out in 1 ms. Furthermore, these smaller CMOS devices that do not require cooling enable faster, easier and less time-consuming installation on different types of beamlines and at different locations.

In summary, our device offers a modern low-cost beam-profile and position monitor that can be used permanently in monochromatic beamlines and should also work for poly-

chromatic beamlines. The device can be paired with existing electronic control systems to enable the automatic positioning/correction of beams and/or sample stages. Furthermore, the device is sealed and therefore has no problems with scattered radiation from windows and slits.

The authors would like to thank Dr W. Bras, S. Nikitenko and the DUBBLE staff for technical support during experiments on BM26 at the ESRF. Many thanks to Dr K. Moon for his advice on the CCD device electronics. NRK and RGvS would also like to thank Dr C. Nave and S. Buffey for their help in the first measurements taken at SRS, Daresbury. This work is supported by grants from the Royal Society (Research Grant No. 22537) and EPSRC (Grant No. GR/R 69860).

References

- Alkire, R. W., Rosenbaum, G. & Evans, G. (2000). *J. Synchrotron Rad.* **7**, 61–68.
- Artemiev, A. N., Latushkin, S., Mikhailov, V., Reznov, V. & Yudin, L. (2002). *Nucl. Instrum. Methods Phys. Res. A*, **477**, 335–339.
- Bergonzo, P., Brambilla, A., Tromson, D., Marshall, R. D., Jany, C., Foulon, F., Gauthier, C., Sole, V. A., Rogalev, A. & Goulon, J. (1999). *J. Synchrotron Rad.* **6**, 1–5.
- Borsboom, M., Bras, W., Cerjak, I., Detollenaere, D., Glastra van Loon, D., Goedtkindt, P., Konijnenburg, M., Levine, Y. K., Munneke, B., Oversluizen, M., van Tol, R. & Vlieg, E. (1998). *J. Synchrotron Rad.* **5**, 518–520.
- Chen, J. R., Ueng, T. S., Hsiung, G. Y., Lin, T. F., Lee, C. T., Tsai, S. L. & Chang, S. L. (1998). *J. Synchrotron Rad.* **5**, 621–623.
- EEV Limited (1999). *A1A-CCD05-30 Series Scientific Image Sensor Issue 4*, <http://e2vtechnologies.com>.
- Hashimoto, Y., Fujita, Y., Morimoto, T., Muto, S., Fujisawa, T., Furukawa, T., Homma, T., Noda, K., Sato, Y., Uchiyama, H. & Yamada, S. (2002). *Proc. EPAC*, pp. 1900–1902.
- Ioudin, L., Mikhailov, V., Reznov, V., Sklyarenko, V., Artemiev, A., Peredkov, S., Rakhimbabev, T., Lemonnier, M., Megtert, S. & Roulliy, M. (1998). *Nucl. Instrum. Methods Phys. Res. A*, **405**, 265–268.
- Koyama, A., Sakaki, S. & Ishikawa, T. (1989). *Rev. Sci. Instrum.* **60**, 1953–1956.
- Sakae, H., Aoyagi, H., Oura, M., Kimura, H., Ohata, T., Shiwaku, H., Yamamoto, S., Sugiyama, H., Tanabe, K., Kobashi, K. & Kitamura, H. (1997). *J. Synchrotron Rad.* **4**, 204–209.
- Schildkamp, W. & Pradervand, C. (1995). *Rev. Sci. Instrum.* **66**, 1956–1959.
- Schulze-Briese, C., Ketterer, B., Pradervand, C., Brönnimann, Ch., David, C., Horisberger, R., Puig-Molina, A. & Graafsma, H. (2001). *Nucl. Instrum. Methods Phys. Res. A*, **467–468**, 230–234.
- Silfhout, R. G. van (1998). *Nucl. Instrum. Methods Phys. Res. A*, **403**, 153–160.
- Silfhout, R. G. van (1999). *J. Synchrotron Rad.* **6**, 1071–1075.